DUCTILE DAMAGE AND CRACK GROWTH ANALYSIS IN 3D STRUCTURES
LIMITATIONS OF CDM APPROACHES

D. Gross and H. Baaser

Institute of Mechanics, Darmstadt University of Technology
Hochschulstrasse 1, D–64289 Darmstadt, Germany
gross@, baaser@mechanik.tu-darmstadt.de

ABSTRACT

Ductile crack initiation and growth is investigated by applying a three–dimensional finite element (FE) analysis in conjunction with a nonlinear damage model. This numerical procedure is formally restricted by the so–called "loss of ellipticity" due to a type change of the differential equations. A time–independent finite strain formulation is applied based on a multiplicative decomposition of the deformation gradient in an elastic and a plastic part leading to an efficient integration scheme. This formulation can be used as a general interface for the implementation of different constitutive models describing "damage" by a scalar quantity in an isotropic manner.
The general problem of describing on the microlevel strongly inhomogenious material behaviour by discretization methods using macroscopic mechanical field quantities, which are microscopic averages, is discussed. Often, typical discretization length scales fall obviously below the intrinsic material length scales, making the sense of the averaging structure of the applied numerical method doubtful.

KEYWORDS

3D–Finite–Element–Simulation, Finite Strain Plasticity, Ductile Damage, Loss of Ellipticity

INTRODUCTION

During the last years applications of models based on continuum damage mechanics (CDM) to ductile fracture mechanics become very popular. The computational evaluation and simulation of damage occurance by different models implemented in the framework of the FEM seems to be very promising, since lots of contributions have followed the first, fundamental publications such as [5], [11] or [7]. It is the common belief that the application of the FE method considering nonlinearities due to advanced constitutive damage models and finite deformations may be capable of simulating classical fracture specimens and test conditions. A well–known disadvantage in the numerical treatment of solid mechanics problems, where softening material behavior occurs, is the so–called *mesh–dependence* of numerical results. In a considerable number of investigations different methods have been proposed to overcome the mesh–dependence of finite element results. The common idea is to introduce a *characteristic* or *internal* length (scale) into the constitutive model or its evaluation, see [2], [3] or [4] and references therein, where a summary of different regularization techniques is outlined.
In this article some limitations and restrictions of ductile damage mechanics analysis in the scope of the finite element method and its nonlinear solution procedures are precisely pointed out at the example of a CT specimen. In order to resolve the highly nonlinear effects of stress and strain concentration occuring near notches, crack tips or due to shear band localization, the numerical discretization in these regions usually is refined without respecting minimal length scales limited by *inhomogenities* on the microscale of the material. Typical physically based length scales of ductile materials such as structural steel or aluminium alloys are in the magnitude of about 50μm – 200μm. But very often length scales resulting from FE discretizations of detailed simulations of damage and crack initiation and growth problems fall below these "natural" barriers. As a consequence, the basic assumptions of continuum mechanics such as continuity of mechanical quantities on the macroscale are violated definitely and the numerical results are highly questionable.
In this study 20–noded brick 3D elements are used with quadratic shape functions along the element edges. As a constitutive model, the ductile damage model of [7] is used. An advantage of this model is the description of material softening behavior due to damage by the influence of solely three material parameters. The second advantage is related to the numerical implementation of the constitutive law by means of an implicit integration scheme. The type of the constitutive equations leads to symmetric tangent material moduli, which is advantageous in computing and storing the matrix expressions. Simultaneously a localization analysis is performed during the iteration on every integration point by evaluation of the so called *localization* or *acoustic tensor* for all possible directions of localization in three dimensions. The fundamental derivation of the acoustic tensor in the case of finite strains is described in [10]. An essential result of this

load, but is restricted until the situation where loss of ellipticity occurs. The investigation is illustrated by a 3D discretization of a CT specimen considering ROUSSELIERs damage model.

3D FINITE ELEMENT FORMULATION

Starting point of any finite element discretization is the weak form of equilibrium $g(\mathbf{u}, \delta\mathbf{u})$ formulated in the current configuration, where $\mathbf{u}$ is the displacement and $\mathbf{t}_L$ are the prescribed tractions acting on the loaded boundary $\partial\mathcal{B}_\sigma$ of the body in the current configuration $\mathcal{B}$. Linearization with respect to the current deformation state and rearrangement leads (with $\mathrm{d}v = J\,\mathrm{d}V$) to the following representation of the element stiffness

$$Dg^{elmt}(\hat{\mathbf{u}}, \delta\mathbf{u}) = \int_{\mathcal{B}_0} J\ (\Delta\boldsymbol{\sigma} + \mathrm{grad}\Delta\mathbf{u}\cdot\boldsymbol{\sigma}) : \mathrm{grad}\,\delta\mathbf{u}\ \mathrm{d}V^{elmt}\,, \tag{1}$$

where $J = \det\mathbf{F}$ and $\mathcal{B}_0$ denotes the reference configuration. For further explanations on the implementation of the consistent linearization of the used algorithm see [9]. The discretization chosen in this paper is based on a 20–node–displacement element formulation with shape functions N_i, $(i = 1, 2, ..., 20)$, so that quadratic functions describe the element edges. As in [6], a $2 \times 2 \times 2$ integration scheme is used, which means an *underintegration* with respect to the quadratic shape functions N_i. It shall be pointed out that no *hourglassing* modes were detected like in the case of an 8–node–displacement element formulation and a $1 \times 1 \times 1$ integration scheme, see [2].

FINITE STRAIN PLASTICITY AND DAMAGE MODEL

Finite strain plasticity

At least in the crack tip region of elastic–plastic solids under sufficiently high load, finite deformations occur where the plastic part of the strains usually is large compared with the elastic part. The framework of multiplicative elastoplasticity is used, which is widely accepted in plasticity.. Its kinematic key assumption is the multiplicative split of the deformation gradient $\mathbf{F} = \mathbf{F}_{el}\cdot\mathbf{F}_{pl}$ into an elastic and a plastic part, providing the basis of a geometrically exact theory and avoiding linearization of any measure of deformation. As a further advantage, fast and numerically stable iterative algorithms, proposed and described in [9], can be used. In the following, only a brief summary of the algorithm in the context of a FE–implementation is given. The essential aspect of the multiplicative decomposition is the resulting additive structure of the current logarithmic principal strains within the return mapping scheme as $\boldsymbol{\epsilon}^{el} = \boldsymbol{\epsilon}^{tr} - \Delta\boldsymbol{\epsilon}^{pl}$. Here, $\epsilon_i = \ln\lambda_i$ $(i = 1, 2, 3)$ and λ_i^2 are the eigenvalues of an elastic trial state, described by the left CAUCHY–GREEN tensor $\mathbf{b}_{el}^{tr}$. The elastic strains $\boldsymbol{\epsilon}^{el}$ are defined by HOOKE's law and the plastic strain corrector $\Delta\boldsymbol{\epsilon}^{pl}$ can be derived by the normality rule of plastic flow. The elastic left CAUCHY–GREEN tensor can be specified with the multiplicative decomposition as $\mathbf{b}_{el} = \mathbf{F}_{el}\cdot\mathbf{F}_{el}^{\mathrm{T}} = \mathbf{F}\cdot\mathbf{C}_{pl}^{-1}\cdot\mathbf{F}^{\mathrm{T}}$, which clearly shows the "connection" between the elastic and plastic deformation measure by the occurance of the plastic right CAUCHY–GREEN tensor $\mathbf{C}_{pl} = \mathbf{F}_{pl}^{\mathrm{T}}\cdot\mathbf{F}_{pl}$. By means of the relative deformation gradient (see [9]) $\mathbf{f} = \partial\mathbf{x}/\partial\mathbf{x}_{n-1} = \mathbf{F}\cdot\mathbf{F}_{n-1}^{-1}$ which relates the current configuration $\mathbf{x}$ to the configuration belonging to the previous time step at t_{n-1}, an elastic *trial*–state $\mathbf{b}_{el}^{tr} = \mathbf{f}\cdot\mathbf{b}_{n-1}\cdot\mathbf{f}^{\mathrm{T}}$ is calculated for the current configuration with frozen internal variables at state t_{n-1}. If the condition $\Phi \leq 0$ (see Eqn. (2)) is fulfilled by the current stress state $\boldsymbol{\tau}$, this state is possible and it is the solution. If, on the other hand, $\Phi \leq 0$ is violated by the trial–state, the trial stresses must be projected back on the yield surface $\Phi = 0$ in an additional step, often called "return mapping".

Rousselier Damage Model

Following the ideas of [1] the stress and strain tensors are decomposed into scalar quantities, which is of advantage for the numerical implementation. Thus, the KIRCHHOFF stress tensor $\boldsymbol{\tau}$ is written as the weighted CAUCHY stress tensor as $\boldsymbol{\tau} = J\,\boldsymbol{\sigma} = -p\mathbf{1} + 2/3\,q^\tau\,\mathbf{n}^\tau$, where $J := \det\mathbf{F} = \mathrm{d}v/\mathrm{d}V = \rho_0/\rho$ and $p = -\tau_{ij}\delta_{ij}/3$ defines the hydrostatic pressure, $q^\tau = \sqrt{3/2\,t_{ij}t_{ij}}$ is the equivalent stress and $t_{ij} = \tau_{ij} + p\delta_{ij}$ are the components of the stress deviator. In this notation, an additional important quantity is the normalized stress deviator $\mathbf{n}^\tau = 3/(2q^\tau)\mathbf{t}$. The second order unit tensor $\mathbf{1}$ is defined as the KRONECKER symbol by its components δ_{ij} in the cartesian frame. In an analogous way the plastic strain rate can be written as $\Delta\boldsymbol{\epsilon}^{pl} = \frac{1}{3}\Delta\varepsilon_p\mathbf{1} + \Delta\varepsilon_q\mathbf{n}^\tau$, where $\Delta\varepsilon_p$ and $\Delta\varepsilon_q$ describe scalar rate quantities which are defined below. The constitutive model used in this study is the damage model proposed by [7]. Here, taking ductile damage processes into account, the yield function is written as

$$\Phi = q^\tau - \underbrace{\sigma_0\left[\frac{\varepsilon_{eqv}^{pl}}{\sigma_0}E + 1\right]^{1/N}}_{\sigma^*} + B(\beta)D\exp(-\frac{p}{\sigma_1}) = 0\,, \tag{2}$$

the damage (softening) behavior by the function $B(\beta)$ and an exponential assumption. Furthermore, D is the YOUNG modulus, σ_0 is the initial yield stress, N is the material hardening exponent, and D and σ_1 are *damage* material parameters. The function $B(\beta)$ is the *conjugate force* to the damage parameter β, defined by $B(\beta) = \sigma_1 f_0 \exp(\beta)/[1 - f_0 + f_0 \exp(\beta)]$. Here, the initial void volume fraction f_0 is the third damage–depending material parameter used in this constitutive set of equations. The macroscopic plastic strain rate $\dot{\boldsymbol{\epsilon}}^{pl}$ is determined by the classical associated flow rule

$$\dot{\boldsymbol{\epsilon}}^{pl} = \dot{\lambda} \frac{\partial \Phi}{\partial \boldsymbol{\tau}} = \dot{\lambda} \left\{ \frac{\partial \Phi}{\partial q^\tau} \frac{\partial q^\tau}{\partial \boldsymbol{\tau}} + \frac{\partial \Phi}{\partial p} \frac{\partial p}{\partial \boldsymbol{\tau}} \right\} . \tag{3}$$

Note that $\dot{\boldsymbol{\epsilon}}^{pl}$ coincides with the plastic increment $\Delta\boldsymbol{\epsilon}^{pl}$ for the algorithmic setting written in the principal axes. The last bracket on the right hand side of (3) shows a further advantage of this formulation following [1], since it is easy to determine the derivatives of Φ with respect to the scalar quantities q^τ and p. It can be seen with (3) that

$$\Delta\varepsilon_p = -\dot{\lambda} \frac{\partial \Phi}{\partial p} \quad \text{and} \quad \Delta\varepsilon_q = \dot{\lambda} \frac{\partial \Phi}{\partial q^\tau} . \tag{4}$$

These two equations allow the algebraic elimination of $\dot{\lambda}$. Thus, the increment of the plastic strain can be expressed by the two scalar quantities $\Delta\varepsilon_p$ and $\Delta\varepsilon_q$. Then the equivalent plastic strain ε^{pl}_{eqv} can be incremented directly by $\Delta\varepsilon_q$. The evolution equation for the damage parameter β is given by $\Delta\beta = \Delta\varepsilon_q D \exp(-\frac{p}{\sigma_1})$, which is obviously dependent on the deviatoric part of the strain rate $\Delta\varepsilon_q$ and the actual hydrostatic pressure p. With this the whole set of the constitutive equations is completed. The evaluation of the material model on the local level of integration points for a given load is realized by an implicit EULER backward integration scheme for the unknowns $\Delta\varepsilon_p$, $\Delta\varepsilon_q$ and $\Delta\beta$. The exact linearization of the set of equations follows the description in [1]. The variational expression

$$\delta\boldsymbol{\tau} = \mathbf{C} : \left(\delta\boldsymbol{\epsilon}^{tr} - \frac{1}{3}\delta\Delta\varepsilon_p \mathbf{1} - \delta\Delta\varepsilon_q \mathbf{n}^\tau - \Delta\varepsilon_q \frac{\partial \mathbf{n}^\tau}{\partial \boldsymbol{\tau}} : \delta\boldsymbol{\tau} \right) \tag{5}$$

leads, after some extended algebraic manipulations as described in [1], to the expressions $\delta\Delta\varepsilon_p$ and $\delta\Delta\varepsilon_q$ and finally to the material modulus for the implicit integration procedure at the end of the considered time interval $[t, t + \Delta t]$.

LOCALIZATION ANALYSIS

Acoustic Tensor

A steady evaluation of the "spatial localization tensor" $\mathbf{Q}$ is performed on every integration point during the iteration to check for material stability. The spatial localization tensor $\mathbf{Q} = \mathbf{n} \cdot \mathbb{D} \cdot \mathbf{n}$ is the contraction of the current fourth order material tensor $\mathbb{D}$ by the spatial surface unit normal vector $\mathbf{n}$ with respect to its second and fourth index. This derivation is introduced in [10] motivated by the assumption of spatially continuous incremental equilibrium across an arbitrary band of discontinuity, which implies that the nominal traction rate inside and outside the band is the same: $\overset{\circ}{\mathbf{t}}(\mathbf{x}^{out}) = \overset{\circ}{\mathbf{t}}(\mathbf{x}^{band})$. With the definition of the nominal traction rate $\overset{\circ}{\mathbf{t}} = J^{-1} \overset{\circ}{\boldsymbol{\tau}} \cdot \mathbf{n}$, the nominal rate of the KIRCHHOFF stress tensor $\overset{\circ}{\boldsymbol{\tau}}$ can be related to the spatial velocity gradient $\mathbf{l} := \dot{\mathbf{F}} \cdot \mathbf{F}^{-1}$ via $\overset{\circ}{\boldsymbol{\tau}} = \mathbb{D} : \mathbf{l}$. These relations become more evident by reformulation of the material rate of the first PIOLA–KIRCHHOFF stress tensor $\dot{\mathbf{P}}$ in terms of the KIRCHHOFF stress tensor $\boldsymbol{\tau}$ into $\dot{\mathbf{P}} = \mathbf{F}^{-1} \cdot \dot{\boldsymbol{\tau}} - \mathbf{F}^{-1} \cdot \mathbf{l} \cdot \boldsymbol{\tau}$. Relating $\dot{\mathbf{P}}$ to the rate of the deformation gradient $\dot{\mathbf{F}}$ via the tangent map $\mathbb{D}^{\mathrm{P}}$, yields

$$\overset{\circ}{\boldsymbol{\tau}} = \dot{\boldsymbol{\tau}} - \mathbf{l} \cdot \boldsymbol{\tau} = \mathbf{F} \cdot \mathbb{D}^{\mathrm{P}} : \dot{\mathbf{F}} , \tag{6}$$

which coincidences with the known *frame–invariant* (*objective*) OLDROYD rate $\overset{\triangledown}{\boldsymbol{\tau}}$ by $\overset{\circ}{\boldsymbol{\tau}} = \overset{\triangledown}{\boldsymbol{\tau}} + \boldsymbol{\tau} \cdot \mathbf{l}^{\mathrm{T}}$. Note that the derivations and the argumentation in [8] — depicted for the case of small strains — about loss of material stability by real or imaginary wave speeds very illustratively denote the term "acoustic tensor" for the double contraction $\mathbf{Q} = \mathbf{n} \cdot \mathbb{D} \cdot \mathbf{n}$ of the material tensor $\mathbb{D}$ by the normal vector $\mathbf{n}$ indicating a possible wave propagation direction. The condition for getting reasonable numerical results is the positive definiteness of the second order tensor $\mathbf{Q}$, which belongs to a positive value of the determinant $q = \det[\mathbf{Q}]$.

Numerical treatment

During the numerical analysis $q = \det[\mathbf{Q}] = \det[\mathbf{n} \cdot \mathbb{D} \cdot \mathbf{n}]$ has to be evaluated for all possible directions $\mathbf{n}$

spherical coordinates with the angles α and β characterizing the longitude and the latitude, respectively. To detect a possible critical direction, where q may vanish, one has to compute $q = \det[\mathbf{Q}] \rightarrow min$ for a set $\{\alpha, \beta\}$. This minimization procedure is synonymous to the evaluation of $\nabla q(\alpha, \beta) = \mathbf{0}$, which can be obtained by a classical NEWTON iteration scheme through

$$\begin{bmatrix}\alpha\\ \beta\end{bmatrix}_{k+1} = \begin{bmatrix}\alpha\\ \beta\end{bmatrix}_{k} - \begin{bmatrix}\frac{\partial^2 q}{\partial \alpha^2} & \frac{\partial^2 q}{\partial \alpha\, \partial \beta}\\ \frac{\partial^2 q}{\partial \alpha\, \partial \beta} & \frac{\partial^2 q}{\partial \beta^2}\end{bmatrix}^{-1} \cdot \begin{bmatrix}\frac{\partial q}{\partial \alpha}\\ \frac{\partial q}{\partial \beta}\end{bmatrix}, \tag{7}$$

and suitable initial conditions, e.g. $[\alpha, \beta]_0^{\mathrm{T}} = [0.1, 0.1]_0^{\mathrm{T}}$, where k indicates the iteration loop number. Because of the large number of operations, the expressions of the related FORTRAN code are obtained by the algebraic manipulation program MATHEMATICA exploiting some advanced methods for code generation.

EXAMPLE AND RESULTS

Model of a CT specimen

As example, a three–dimensional model of a CT specimen discretized by 20–node solid elements as shown in Fig. 1(1) is examined. Due to symmetry, just a quarter of the structure is modeled, for length dimensions

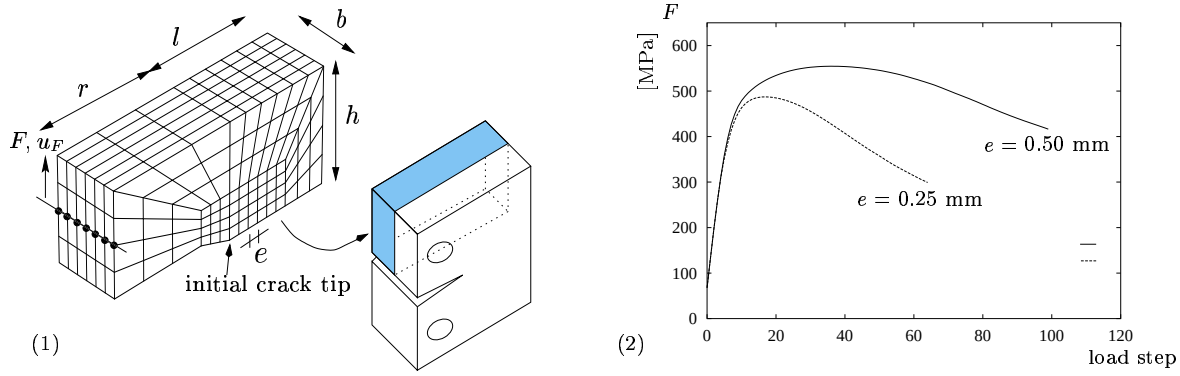

Figure 1: Model of CT specimen and typical load–deflection curve for different discretizations

see Tab. 1. The loading is applied by a prescribed displacement u_F (by 0.01 mm/step) of the nodes lying on the marked line, see Fig. 1(1). The chosen discretization is characterized by the typical element edge length e in front of the crack tip. In this investigation the element edge lengths $e = 0.50$ mm and $e = 0.25$ mm are used. Additionally the typical mesh sensitive results for a classical, local FE simulation using different discretizations are plotted as load–deflection curve in Fig. 1(2), where obviously the dependence of the reaction force on the finite element mesh can be seen. The set of material parameters used is shown in Tab. 1, where the first four parameters can be obtained by simple tensile tests, and D, σ_1 and f_0 are responsible for the damage representation of the constitutive model.

Table 1: MATERIAL PARAMETERS

E [MPa]	ν	σ_0 [MPa]	N	D	σ_1 [MPa]	f_0	r [mm]	l [mm]	b [mm]	h [mm]
210000	0.2	460	7	3	300	0.01	6	5	3	5

Results

A result for the load–displacement curves for different discretizations is plotted in Fig. 1(2) and can also be found in [3]. The mesh sensitivity is obvious, if no additional regularization technique is applied. In the following, we concentrate on computations resulting from the evaluation of the localization tensor $\mathbf{Q}$ and its determinant. The representation of the results is focussed on observations of the FE–integration point being located directly in front of the crack tip in the center of the specimen, which is the highest loaded point with the most increased damage parameter. Fig. 2 shows the normalized determinant of $\mathbf{Q}$ vs. the two spatial angles α and β parameterizing the normal vector $\mathbf{n}$ in each case by 20 steps (ROUSSELIER parameter set of Tab. 1 and $e = 0.50$ mm). Displayed is the situation for load steps 2, 4 and 8 ($u_F = 0.02, 0.04, 0.08$ mm), which represents directly the situation before the onset of localization ($q \rightarrow 0$). Obviously one can recognize the decrease of $q/|Q_{11}Q_{22}Q_{33}|$ during load steps 2–8.

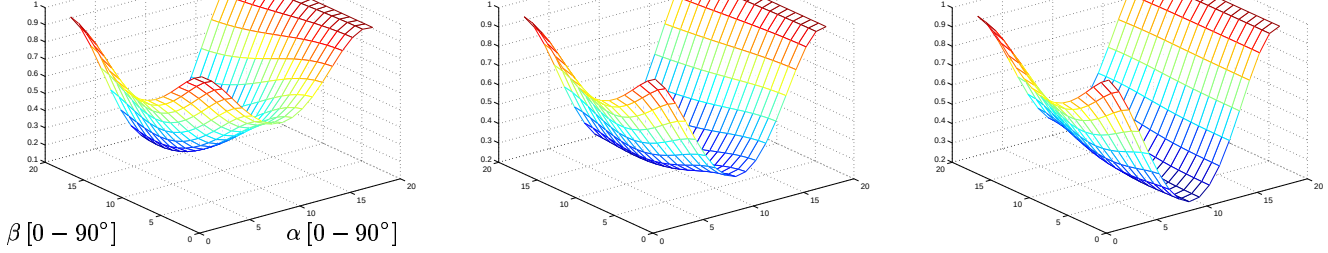

load step 2, $u_F = 0.02$ mm | load step 4, $u_F = 0.04$ mm | load step 8, $u_F = 0.08$ mm

Figure 2: Evaluation of the acoustic tensor

Because of the numerical costs determining these quantities during the iteration, we apply a NEWTON iteration scheme following Eqn. (7) for finding the minimum of these surfaces. For the integration point of interest, Fig. 3(1) shows the value of det $[\mathbf{Q}]$ vs. 30 load steps for two different discretizations with $e = 0.50$ mm and $e = 0.25$ mm and ROUSSELIER material, respectively. Additionally, the situation for a standard (non damaging) VON MISES material with the same power–hardening law σ^* and $e = 0.50$ mm is plotted. As expected, for the VON MISES material, the values of q decrease rapidly during the load incrementation over 30 steps, but never reach $q = 0$ indicating a possible localization.
In contrast, the curves for the ROUSSELIER damage material representation show precisely a zero–crossing and thus a localization occurance. Again, the mesh sensitivity is obvious through the results for $e = 0.25$ mm at load step 4, while the discretization with $e = 0.50$ mm reaches zero at load level 9. In Fig. 3(2) the equiv-

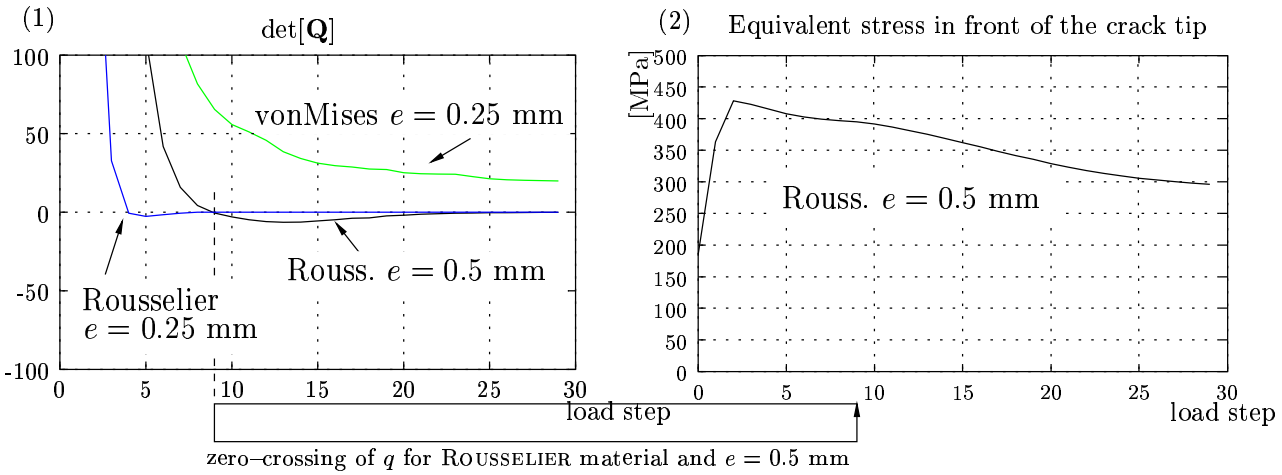

Figure 3: Determinant of acoustic tensor $\mathbf{Q}$ and equivalent stress in front of the crack tip

alent stress of the integration point in front of the crack tip is plotted vs. the applied load steps for the ROUSSELIER material and $e = 0.50$ mm. Note that the equivalent stress at the critical load level 9 ($u_F = 0.09$ mm) appears in the decreasing part of the load curve obviously after reaching the peak load.
Fig. 4 depicts the contours of integration points, where the determinant of the acoustic tensor reaches zero for the load steps 10, 20 and 30 in front of the crack tip. The contour lines in crack propagation direction are plotted over the discretized width b of the specimen using $e = 0.50$ mm and the ROUSSELIER material set of Tab. 1 demonstrating local loss of ellipticity in front of the crack tip during the computation. It should be emphasized, that the contour lines $q = 0$ must not be mixed up with the contour lines of lost load carrying capacity (crack growth) defined by a critical damage parameter. These crack growth contours follow the $q = 0$ contours far behind (at higher load steps), indicating that they are determined in inadmissible situations. These results show impressingly the close limits of the continuum damage mechanics using the FE method without additional regularization avoiding a type change of the leading differential equation. Mesh refinements resulting in the typical mesh sizes in the magnitude of the intrinsic material length scales can not represent the real, potentially inhomogenious, material structure on the microlevel.

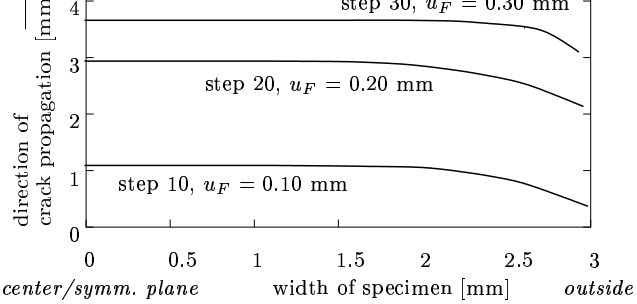

Figure 4: Contours of integration points on the ligament reaching $q = 0$ for load steps 10, 20, 30 using the ROUSSELIER material set and $e = 0.50$ mm

SUMMARY

In this contribution we present a study on ductile damage analysis by a 3D simulation of CT specimen using the ROUSSELIER damage model combined with a 3–dimensional finite element formulation based on 20–node–solid elements. The main attention is put to the limitations of the finite element method discretizing mechanical field equations by piecewise continuous functions, which are used to represent inhomogenious constituents of material on the microscale.
Typical FE analyses, resolving the situations in front of crack tips or in shear band regions as detailed as possible, are known to produce very mesh sensitive results because of the changing type of the basic differential equations. This "loss of ellipticity" is checked by a steady evaluation of the acoustic tensor and a stop of the overall computation reaching such a point of stability. It is worth mentioning that this critical situation is reached very early during the nonlinear iteration process, so that the subsequently determined numerical results become questionable, if no method of regularization is applied.

REFERENCES

[1] N. Aravas. On the numerical integration of a class of pressure–dependent plasticity models. *International Journal for Numerical Methods in Engineering*, 24:1395–1416, 1987.

[2] H. Baaser and D. Gross. Damage and strain localisation during crack propagation in thin–walled shells. In A. Bertram and F. Sidoroff, editors, *Mechanics of Materials with Intrinsic Length Scale*, number ISBN 2-86883-388-8, pages 13–17, Magdeburg, Germany, 1998A. EDP Sciences. Journal de Physique IV, **8**.

[3] H. Baaser and D. Gross. 3D Nonlocal Simulation of Ductile Crack Growth — A Numerical Realization. *European Journal of Finite Elements*, 2001. To appear.

[4] H. Baaser and V. Tvergaard. A new algorithmic approach treating nonlocal effects at finite rate-independent deformation using the ROUSSELIER damage model. *submitted to Computer Methods in Applied Mechanics and Engineering*, 2000. see also DCAMM Report 647, TU Denmark, Lyngby.

[5] A.L. Gurson. Continuum theory of ductile rupture by void nucleation and growth: Part I - yield criteria and flow rules for porous ductile media. *Journal of Engineering Materials and Technology*, 99:2–15, 1977.

[6] K.K. Mathur, A. Needleman, and V. Tvergaard. Ductile failure analyses on massively parallel computers. *Computer Methods in Applied Mechanics and Engineering*, 119:283–309, 1994.

[7] G. Rousselier, J.-C. Devaux, G. Mottet, and G. Devesa. A methodology for ductile fracture analysis based on damage mechanics: An illustration of a local approach of fracture. *Nonlinear Fracture Mechanics*, 2:332–354, 1989.

[8] H.L. Schreyer and M.K. Neilsen. Analytical and numerical tests for loss of material stability. *International Journal for Numerical Methods in Engineering*, 39:1721–1736, 1996.

[9] J.C. Simo. Algorithms for static and dynamic multiplicative plasticity that preserve the classical return mapping schemes of the infinitesimal theory. *Computer Methods in Applied Mechanics and Engineering*, 99:61–112, 1992.

[10] P. Steinmann, R. Larsson, and K. Runesson. On the localization properties of multiplicative hyperelasto–plastic continua with strong discontinuities. *International Journal of Solids and Structures*, 34(8):969–990, 1997.

[11] V. Tvergaard. Material failure by void growth to coalescence. *Advances in Applied Mechanics*, 27:83–151, 1989.